Cell Reports

Cryo-EM structure of the SARS-CoV-2 Omicron spike

Graphical abstract
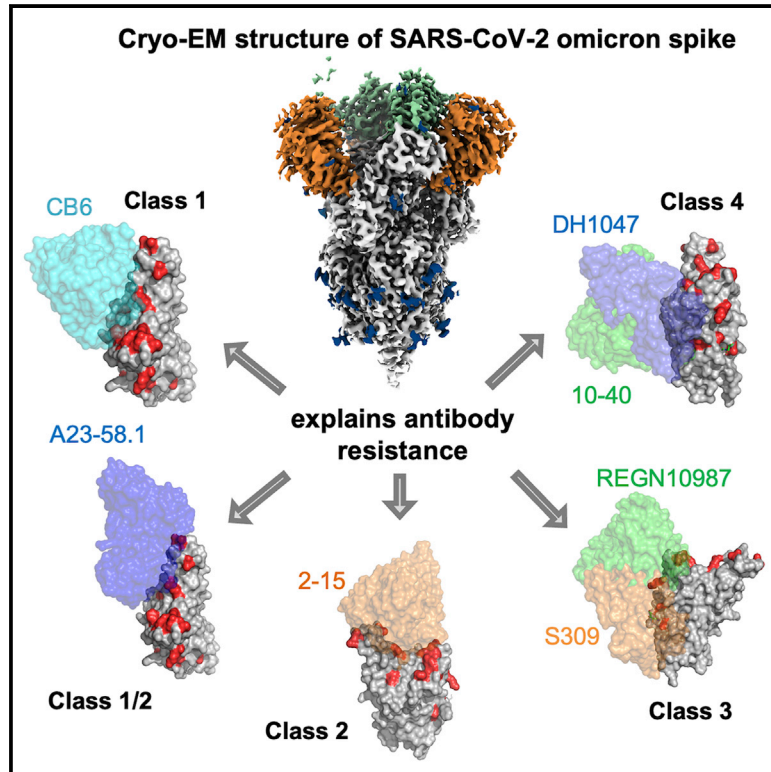
Authors

Gabriele Cerutti, Yicheng Guo,
Lihong Liu, ..., David D. Ho,
Zizhang Sheng, Lawrence Shapiro

Correspondence

dh2994@cumc.columbia.edu (D.D.H.),
zs2248@cumc.columbia.edu (Z.S.),
lss8@columbia.edu (L.S.)

In brief

Cerutti et al. report the cryo-EM structure
of the SARS-CoV-2 Omicron spike in its
ligand-free form. The structure elucidates
the effect of the mutations on the global
and local conformation of spike and
explains the antibody resistance to the
Omicron variant.

Highlights

- SARS-CoV-2 Omicron spike exclusively adopts a 1-RBD-up conformation

- Omicron substitutions alter conformation and mobility of the RBD

- A subset of Omicron mutations changes the local conformation of spike

- The structure reveals the basis of antibody neutralization escape

CellPress

Report

Cryo-EM structure of the SARS-CoV-2 Omicron spike

Gabriele Cerutti,[1,2,5] Yicheng Guo,[2,3,5] Lihong Liu,[3,5] Liyuan Liu,[4,5] Zhening Zhang,[1] Yang Luo,[3] Yiming Huang,[4] Harris H. Wang,[4] David D. Ho,[3,*] Zizhang Sheng,[3,*] and Lawrence Shapiro[1,2,3,6,*]

[1]Department of Biochemistry and Molecular Biophysics, Columbia University, New York, NY 10032, USA
[2]Zuckerman Mind Brain Behavior Institute, Columbia University, New York, NY 10027, USA
[3]Aaron Diamond AIDS Research Center, Columbia University Vagelos College of Physicians and Surgeons, New York, NY 10032, USA
[4]Department of Systems Biology, Columbia University Vagelos College of Physicians and Surgeons, New York, NY 10032, USA
[5]These authors contributed equally
[6]Lead contact
*Correspondence: dh2994@cumc.columbia.edu (D.D.H.), zs2248@cumc.columbia.edu (Z.S.), lss8@columbia.edu (L.S.)
https://doi.org/10.1016/j.celrep.2022.110428

SUMMARY

The recently reported B.1.1.529 Omicron variant of severe acute respiratory syndrome coronavirus-2 (SARS-CoV-2) includes 34 mutations in the spike protein relative to the Wuhan strain, including 15 mutations in the receptor-binding domain (RBD). Functional studies have shown Omicron to substantially escape the activity of many SARS-CoV-2-neutralizing antibodies. Here, we report a 3.1 Å-resolution cryoelectron microscopy (cryo-EM) structure of the Omicron spike protein ectodomain. The structure depicts a spike that is exclusively in the 1-RBD-up conformation with high mobility of RBD. Many mutations cause steric clashes and/or altered interactions at antibody-binding surfaces, whereas others mediate changes of the spike structure in local regions to interfere with antibody recognition. Overall, the structure of the Omicron spike reveals how mutations alter its conformation and explains its extraordinary ability to evade neutralizing antibodies.

INTRODUCTION

Severe acute respiratory syndrome coronavirus 2 (SARS-CoV-2) emerged as a human pathogen in 2019 in Wuhan, China, causing a disease now known as coronavirus disease 19 (COVID-19), which is characterized by fever, acute respiratory illness, and pneumonia (Callaway et al., 2020; Cucinotta and Vanelli, 2020; Zhou et al., 2020). At the time of writing this article, more than 274 million infections had been reported worldwide, with over 5 million deaths (https://arcg.is/0fHmTX, 2021). Numerous variants have been discovered through sequencing over the past 2 years, with some major lineages designated as variants of concern (VOCs) due to increased transmissibility, disease severity, resistance to neutralizing antibodies elicited by vaccines, or reduced efficacy of treatments (Planas et al., 2021a; Washington et al., 2021). These VOCs are designated alpha, beta, delta, and gamma by the World Health Organization, each of which contains a characteristic set of mutations. The Omicron (B.1.1.529) VOC, first detected in southern Africa in November 2021, has spread rapidly to over 60 countries. The astonishingly high transmission rate (R0 >3) and short doubling time (2–3 days) of Omicron cases suggests it could soon become dominant (Burki, 2021). The alarming number of mutations in the spike protein (34), including at least 15 in the receptor-binding domain (RBD), the primary target for neutralizing antibodies, results in substantially compromised efficacy of vaccines and therapeutic antibodies (Cameroni et al., 2021; Cao et al., 2021; Carreño et al., 2021; Liu et al., 2021a; Planas et al., 2021b). Elucidating the structural basis of viral escape becomes a high priority for understanding viral evolutionary pathways and developing new therapeutics.

SARS-CoV-2 utilizes a highly glycosylated spike protein (S) to mediate entry into host cells. S, a class I fusion protein, forms a trimer that adopts a metastable prefusion conformation that undergoes large structural rearrangements in fusion of the host and viral cell membranes (Bosch et al., 2003; Shang et al., 2020). Host cell angiotensin-converting enzyme 2 (ACE2) receptor binding is thought to destabilize the prefusion trimer, leading to shedding of the S1 subunit and transition of S2 to an elongated helical postfusion conformation (Benton et al., 2020; Cai et al., 2020; Hoffmann et al., 2020; Wang et al., 2020). The RBD of S1 undergoes conformational motions between an "up" state where the ACE2 receptor-binding site is accessible, and a "down" state where it is hidden (Walls et al., 2020; Wrapp et al., 2020).

Neutralizing antibodies most often target the domains at the top of the spike: RBD (Barnes et al., 2020; Brouwer et al., 2020; Cao et al., 2020; Cerutti et al., 2021c; Chen et al., 2020; Ju et al., 2020; Liu et al., 2020b; Pinto et al., 2020; Rapp et al., 2021; Shi et al., 2020; Tortorici et al., 2020; Zost et al., 2020), and N-terminal domain (NTD) (Cerutti et al., 2021a, 2021b; Chi et al., 2020; McCallum et al., 2021a; Suryadevara et al., 2021). The large number of mutations in Omicron has raised questions about its evolutionary origin. Some have proposed that it developed in a chronically infected individual with an impaired immune response, whereas others think it developed in parallel with other variants in a population not monitored by sequencing (Kupferschmidt, 2021). Mutations in VOCs accumulate mainly in the S protein. Omicron has 15, eight, and 11 mutations in RBD, NTD, and S2 subunits
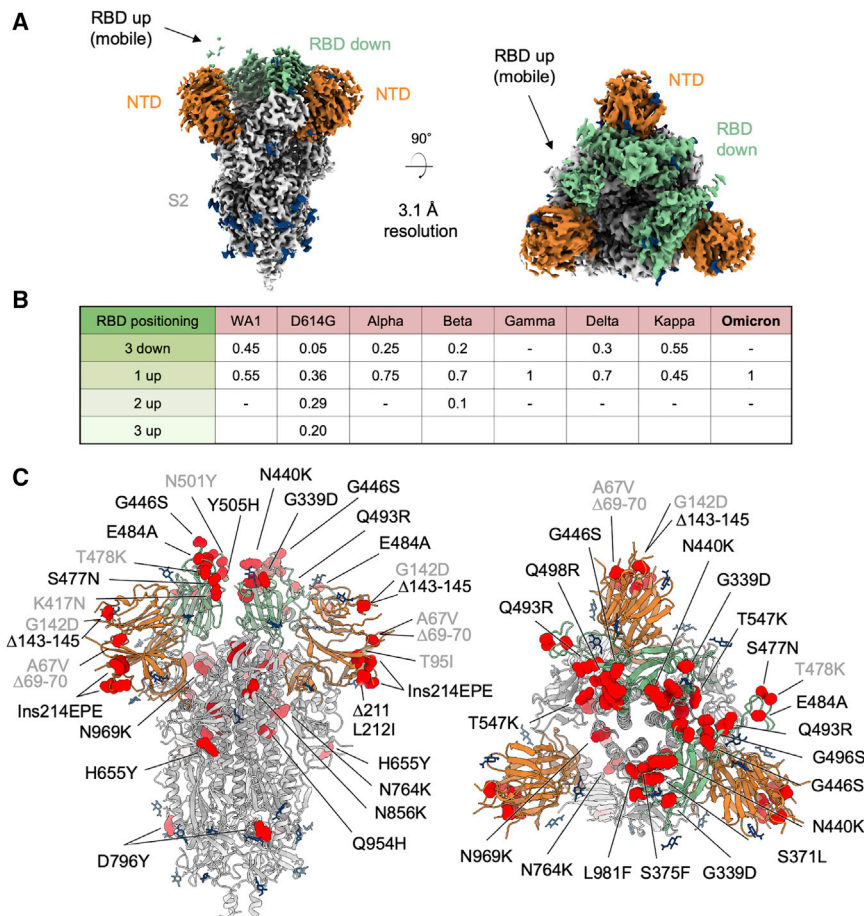
RBD positioning	WA1	D614G	Alpha	Beta	Gamma	Delta	Kappa	**Omicron**
3 down	0.45	0.05	0.25	0.2	-	0.3	0.55	-
1 up	0.55	0.36	0.75	0.7	1	0.7	0.45	1
2 up	-	0.29	-	0.1	-	-	-	-
3 up		0.20						

have previously been used to stabilize the spike in its prefusion form (Walls et al., 2020; Wrapp et al., 2020), and a C-terminal His tag. The protein was expressed in Expi293 cells and purified by His-tag affinity chromatography, and this protein was used for the preparation of cryo-EM grids. The spike appeared to show a slight preferred orientation on the cryo-EM grids, so we collected data with a 30° tilt angle. We collected and processed 13,695 cryo-EM movies to obtain a 3D reconstruction at 3.1 Å resolution (Figures 1A, S1, and S2, Table S1).

The overall structure is similar to the Wuhan spike, with only a 1-RBD-up conformation identified through *ab initio* map generation and 3D classification. The electron density for the RBD in the up position is blurred compared with the density of the RBDs in the down position (Figure 1A). To investigate this behavior, we performed 3D variability analysis, a procedure that allows visualization of structural heterogeneity, like partial occupancy and molecular motions, by sampling the heterogeneity of a 3D reconstruction in 3D linear subspace models (variability components) (Punjani and Fleet, 2021). The main variability component observed within the final particle set showed an oscillatory motion for the RBD up (Figure S3), suggesting that the RBD up exists in multiple conformations. The electron densities for the two RBDs down were not equivalent, with the best RBD density observed for protomer B (Figure S1E).

The single 1-RBD-up conformation observed for Omicron is also typical of the gamma variant (Wang et al., 2021a; Zhang et al., 2021b), while for other variants an equilibrium of different states has been reported (Figure 1B) (Gobeil et al., 2021; Yurkovetskiy et al., 2020; Zhang et al., 2021a, 2021b). Specifically, the blurred density for the RBD up observed in Omicron spike was reported for the alpha variant (Gobeil et al., 2021).

Most of the Omicron mutations were visible in the cryo-EM structure and their location in the context of spike is depicted in Figure 1C. Mutations Δ69–70 (NTD), S373P (RBD), N679K,

respectively, with six of the 34 mutations observed in other VOCs or variants of interest. The RBD mutations include G339D, S371L, S373P, S375F, K417N, N440K, G446S, S477N, T478K, E484A, Q493R, G496S, Q498R, N501Y, and Y505H. Some of these mutations have known functional consequences, such as K417N, S447N, E484A, and Q493R, which contribute to immune escape (Harvey et al., 2021; Wang et al., 2021b), and N501Y which contributes to higher infectivity (Tian et al., 2021). However, other Omicron mutations in RBD and other domains have unknown functional impact, individually or in combination.

Here we present the cryoelectron microscopy (cryo-EM) structure of the Omicron spike, which adopts an exclusively 1-up RBD conformation. The overall architecture of the spike is conserved, but the mobility of RBDs appears increased over other variants. Surface differences appear to be localized around sites of antibody recognition, with serious implications for immune evasion.

RESULTS

Cryo-EM structure of Omicron spike

For structure determination, we produced a soluble version of the Omicron spike corresponding to residues 1 to 1,208 of the ectodomain, and including two proline mutations in S2 that

and P681H (proximal to the S1/S2 cleavage site) belonged to flexible regions that could not be resolved in the cryo-EM structure. The remaining 30 mutations were visible in the cryo-EM map although the side chains of mutated residues G142D, G339D, S477N, T478K, and G496S were not resolved (Figure S2, Table S2). The RBD mutations are mostly clustered near the inter-protomer RBD-RBD interface and many of them overlap with the ACE2-binding site, while the NTD mutations are located in the flexible loops distal from the trimer axis. The S2 mutations are mostly located at the top of the subunit, at the interface with S1.

Similarity and difference between Omicron and D614G spike

To evaluate whether the Omicron mutations induce overall orientation changes among spike domains, we superimposed the structures of Omicron variant to the D614G wild type (WT) with 1-up RBD (PDB: 7KRR) (Figure 2A). The comparison revealed an overall root-mean-square deviation (RMSD) of 1.1 Å and 0.6 Å for S1 and S2 subunits respectively. The measured distance between NTDs of the three protomers showed that the NTD from protomer A (NTD$_A$), which has an RBD up, is 5 Å closer to the NTD of protomer B (NTD$_B$) than that of the D614G spike (Figure 2B). We also observed that the S2 helix bundle (residues 988 to 1,033) has a shorter distance and increased buried accessible surface area (bASA) between protomers than the WT spike (Figure 2C and Table S3).

We then determined the center of mass (COM) for NTD, NTD′, SD2, SD1, and RBD and used COMs to calculate angles between these domains. The result revealed that protomer A has a smaller angle between NTD′, SD2, and SD1, while the angles between other domains are highly similar to the WT spike (Figure 2D). The angles between the five domains in protomers B and C have no difference compared with the WT. We then measured the bASA between the above domains and found that almost every domain-domain interface bASA increases slightly in Omicron compared with the WT (Table S3). Remarkably, NTD has a 3-fold increased bASA with adjacent RBD, coupled to a 2-Å reduced distance between RBD and NTD through the orientation change in NTD. In summary, our analyses showed increased inter-domain interactions of the Omicron spike.

Effects of Omicron mutations on spike conformation

We next mapped the Omicron mutations to the spike structure and assessed their potential effects on spike conformation. The majority of the RBD mutations are located in the receptor-binding motif (RBM), inner-side, and outer-side epitope regions (Figure 3A). The superimposition of the Omicron and WT RBDs showed an RMSD of 0.75 Å. We then calculated Cα distance for each RBD residue between Omicron and WT, and observed that six mutations (S371L, S373P, S375F, G446S, S477N, and T478K) are located at regions with Cα distance larger than 2 Å (Figure 3B), suggesting that these mutations may account for the conformational change in the Omicron RBD. In particular, we observed that mutations S371L, S373P, and S375F not only alter the conformation of loop 371–376 but also result in the motion of helix 365–370 closer to helix 337–343, which

may alter the conformation of the N-linked glycosylation at N343 (Figure 3C left panel). The formation of new hydrogen bond networks by mutations G446S, G496S, Q498R, and N501Y stabilize loop 443–451 to a new conformation (Figure 3C right panel).

The majority of NTD mutations are located at the antigenic supersite targeted by most NTD-directed neutralizing antibodies. Our Omicron structure revealed substantial conformational changes in the NTD supersite (Figure 3D left and middle panels). We also determined part of the N3 loop with G142D and Δ143–145 (Figure 3D right panel). In addition, in the two RBD-down protomers, we observed Omicron S2 mutations N764K and N856K to form new hydrogen bonds with SD1 and SD2 domains from adjacent protomers respectively (Figure 3E). Two conserved residues nearby these mutations also form additional hydrogen bonds in Omicron spike (Figure S4C). Because both SD1 and SD2 undergo a substantial rearrangement when the RBD switches to the up conformation, these interactions may help to stabilize the RBD in the down conformation by locking SD1 and SD2, an effect similar to other S2 mutations (Gobeil et al., 2021).

Mechanisms of antibody escape

Previous studies showed that the Omicron variant impairs neutralization of numerous RBD- and NTD-directed antibody classes that represent convergent human antibody response to SARS-CoV-2 (Cameroni et al., 2021; Cao et al., 2021; Liu et al., 2021a; Planas et al., 2021b). To understand the structural basis of immune evasion by Omicron, we superimposed the published structures of SARS-CoV-2 antibody/RBD or NTD complexes to the Omicron RBD or NTD and identified mutations substantially contributing to neutralization reduction. Previous studies showed consistently that K417N and Q493R impair neutralization of class 1 and 2 antibodies (Amanat et al., 2021; Wang et al., 2021b). Our structural analysis revealed that the impairment of neutralization is probably through steric clash and reduced polar interactions (Figures 4A and S5A). E484A reduces polar interactions with class 2 antibodies. For class 3 antibodies, G446S induces steric clashes with CDRH3. The Omicron structure also revealed that the conformational changes in loop 443–451 enhance steric hindrance (Figure S5B left panel). For class 4 antibodies, the altered conformation of helix 365–370 and loop 371–376 reduces the interaction with the CDRH3 tip of class 4 antibodies (Figures 4B and S5B right panel), which may increase the entropy of the epitope/paratope interaction. In addition, the mutations at 371, 373, and 375 are likely to impair recognition of quaternary epitope recognizing class 1 or 2 antibodies (Figure S5C). The NTD point mutations and deletions alter the antigenic supersite substantially (Figure 4C), abolishing neutralization by most NTD-directed neutralizing antibodies (Liu et al., 2021b).

DISCUSSION

We report the cryo-EM structure of the SARS-CoV-2 spike of the highly transmissible Omicron variant, which includes an unprecedented number of mutations and achieves an unprecedented level of antibody escape. While the structure is similar overall
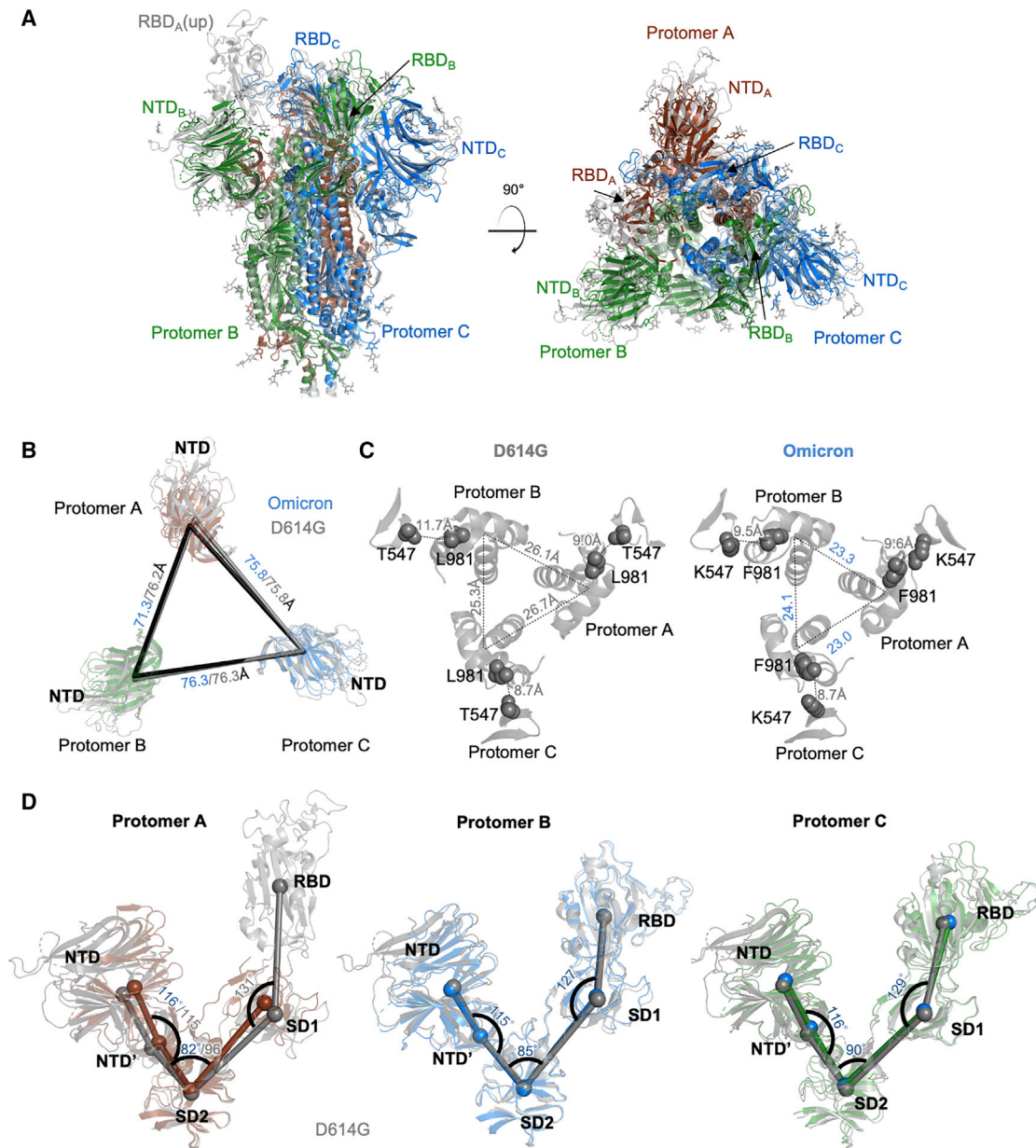
Figure 2. Structural comparison of SARS-CoV-2 Omicron spike with D614G WT
(A) Superposition of Omicron spike with D614G spike. The S2 subunit is used for superimposition.
(B) Distance between NTDs of Omicron spike and D614G spike.
(C) The inter-protomer distance between S2 helices in Omicron is shorter than that observed in D614G spike.
(D) Measured angles between NTD, NTD′, SD2, SD1, and RBD showed that protomer A with an up-RBD has altered angles between NTD′, SD2, and SD1. The two protomers with RBDs down show similar domain orientation. Thus, only angles of the Omicron spike are shown. See also Table S3.

to the D614G spike, it exists in an all 1-RBD-up conformation with high mobility of RBD. Conformational differences associated with Omicron mutations occlude known antibody-binding sites and thus are also likely to contribute to antibody evasion.

The observed 1-RBD-up spike conformation may have evolutionary advantage. For example, the cryptic epitopes, which are only available in the RBD up and are recognized by antibody classes 1 and 4, have a lower frequency of exposure

compared with the WT. Together with high mobility of the RBD up and mutations, the Omicron spike can shed off recognition by dominant human antibodies elicited by infection and vaccination. Since many antibodies recognize two RBDs up simultaneously to enhance neutralization through avidity, the reduced number of RBDs up may decrease this effect (Liu et al., 2020a; Rapp et al., 2021). In this study, we observed that S2 mutations N764K and N856K may play a role in
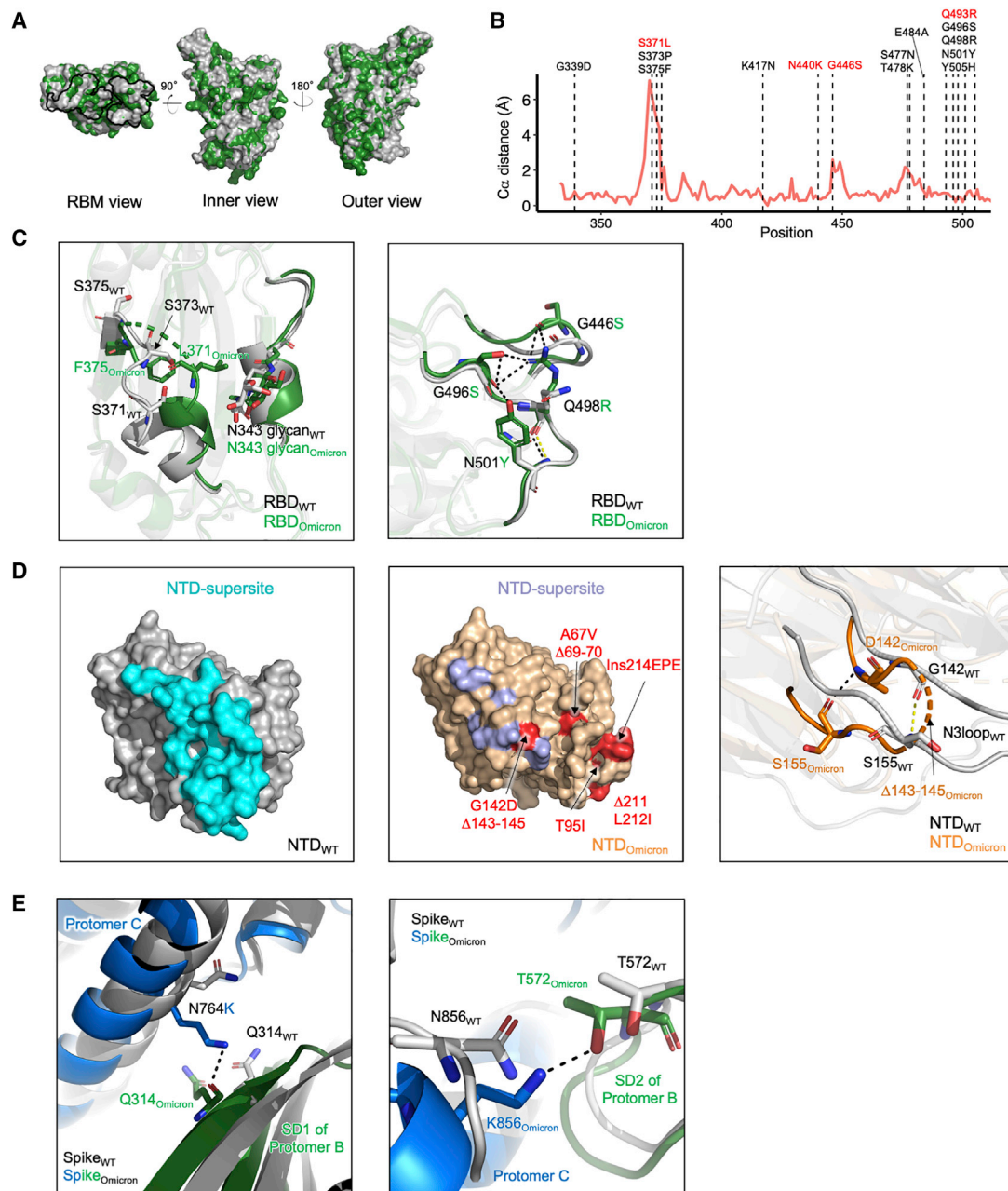
Figure 3. Omicron spike mutations alter local conformation and polar interaction pattern

(A) Superposition of Omicron RBD with WT RBD. The Omicron RBD is colored in green and WT RBD in gray. The dark line shows the footprint of the RBM.

(B) Per-residue Cα distance between Omicron and WT RBD. RBD mutations in Omicron are labeled. The Omicron-specific mutations labeled in red resulted in dramatic and broad antibody neutralization resistance.

(C) Details of conformation changes in Omicron RBDs. Left: 367–375 conformation change. Right: 444–448 loop conformation change. Black and yellow dashed lines show hydrogen bonds in Omicron and WT RBDs respectively.

(D) Comparison of Omicron and WT NTD. Left: structure for WT NTD with the NTD supersite colored cyan. Middle: structure for Omicron NTD; the blue residues show the NTD supersite on Omicron, the red residues labeled the Omicron mutations. Right: details of N3 loop change in Omicron compared with WT.

(E) S2 mutations N764K and N856K in Omicron form new polar interactions with SD2 and SD1 from adjacent protomers respectively. See also Figure S4.

stabilizing RBDs in the down conformation through additional interactions with SD1 and SD2 domains. L547K and L981F are close to the RBD in the down conformation of adjacent pro-tomers (Figure S4D), which may also contribute by altering S2/

RBD interactions. The four mutations are also close to the S2 helix bundle (Figures 2D and S4D), and may contribute to the observed S2 conformational change, but the mechanism re-mains unclear.
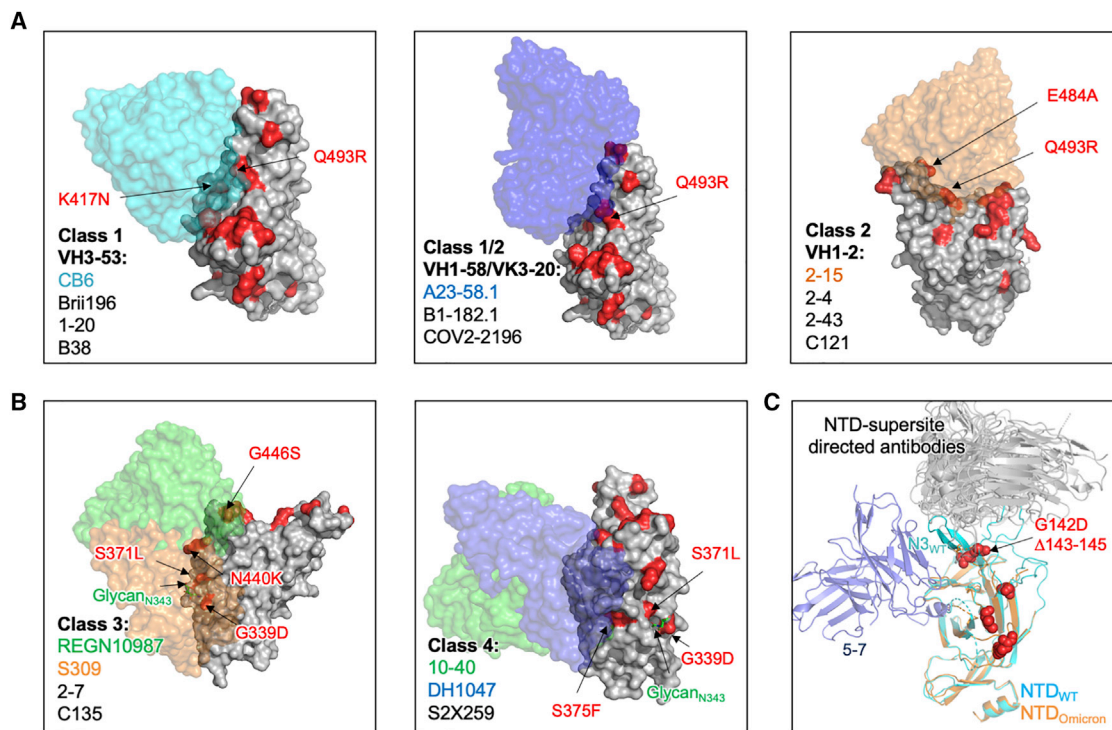
Figure 4. Structural basis of neutralizing antibody escape by Omicron

(A) Surface diagram of class 1 and 2 antibodies bound to RBD. Left: VH3-53-derived antibodies with CB6 as an example (PDB: 7C01). Middle: VH1-58/VK3-20-derived antibodies with A23-58.1 (PDB: 7LRS)-binding mode shown. Right: VH1-2-derived antibody with 2-15 (PDB: 7L57)-binding mode shown. Mutations in Omicron RBD are colored in red.

(B) Surface diagram of the class 3 and 4 antibodies bound to Omicron RBD, antibody REGN10987 (PDB: 6XDG), S309 (PDB: 6WPT), 10–40 (PDB: 7SD5), and DH1047 (PDB: 7LD1) are shown.

(C) Cartoon diagrams of the Omicron and WT NTDs in complex with antigenic supersite-directed antibodies and 5-7 (PDB: 7RW2). Omicron mutations are shown as red spheres. See also Figure S5.

A convergent antibody response in humans results in distinct spike regions subject to antibody neutralization. Antibodies directed against RBD embody one of the primary immune defenses against SARS-CoV-2. Omicron spike contains 15 mutations in RBD, many overlapping the recognition surfaces of neutralizing antibodies. Compared with other VOCs, Omicron also accumulated mutations extensively within and surrounding the RBM. These mutations lead to the escape of antibodies of all major structural classes—including classes 1, 2 and 3—which has been observed to a lesser extent with other VOCs. In contrast, Omicron has two unique clusters of mutations in the RBD. One cluster is G446S, G496S, and Q498R. This cluster of mutations cooperatively alter the loop 443–451 recognized by classes 1, 2, and 3 antibodies, suggesting the result of strong immune selection pressure. The second mutation cluster is S371L, S373P, and S375F, which alter the conformation of loop 371–376 and helix 365–370. These mutations allow Omicron to evade class 4 antibodies (Saunders et al., 2021), directed to a highly conserved region on the "side" of RBD, which has so far been observed with no other VOC. Besides, two additional classes of antibodies, quaternary epitope recognizing class 1 and 2 antibodies (e.g., 2–43 and S2M11) (Rapp et al., 2021; Tortorici et al., 2020) and S309-like class 3 antibodies (Andreano et al.,

2021), are also impaired by the three mutations. In addition, helix 365–370 tends to have stronger interaction with the base of the N-linked glycosylation at N343, which plays roles in stabilizing two adjacent RBDs down (Rapp et al., 2021). Together with G339D, these mutations may alter the orientation of the N-linked glycosylation at N343, which may affect antibody binding to adjacent epitope regions.

NTD-directed antibodies also constitute an important defense, with most neutralizers directed to a single antigenic supersite (Cerutti et al., 2021b; McCallum et al., 2021a). Similar to other VOCs, Omicron contains mutations and deletions directly within loops of the supersite, providing a structural explanation for escape from this major class of antibodies (McCallum et al., 2021b). Overall, this is consistent with the idea that Omicron evolved in response to the immune pressure of neutralizing antibodies.

The conformational and electrostatic changes induced by RBD mutations help to understand the enhanced ACE2-binding affinity by the Omicron spike (Lan et al., 2022; Mannar et al., 2021; Yin et al., 2021). The electrostatic analysis revealed the RBM to contain more positive charges than the Wuhan strain (Figure S4E). The increased positive electrostatic potential resulting from Omicron mutations T478K, Q493R, and Q498R

CellPress
OPEN ACCESS

may thus result in an increased affinity for the negatively charged residues on ACE2.

In summary, this study reports the structural impact of mutations emerged with the Omicron variant on the architecture of SARS-CoV-2 spike. The cryo-EM structure reveals the details of Omicron spike conformational modulation and immune evasion in the context of the natural evolution of the virus. As the Omicron mutations overlap with epitopes of neutralizing antibodies, our structural analysis explains the antibody resistance and informs the identification of effective therapeutic and prophylactic strategies.

Limitations of the study

The cryo-EM reconstruction reported in this paper showed a very blurred density for the RBD in the up conformation, not modeled in the deposited coordinates. The two RBDs down were not equivalent in terms of map quality, with the RBD in protomer B showing higher resolution. Poor EM density was also observed for other regions: residues 14–25, 69–77, 144–152, 177–185, 246–259, 678–688, 828–838 (protomer A), and 828–849 (protomer B and C) were not visible in the cryo-EM map. Mutations G142D, E214a, E214c, G339D, S447N, T478K, and G496S were modeled as stubs in the associated coordinates. Mutations S373P, N679K, and P681H were not modeled since they were not visible in the map.

The effect of the mutations on the antigenicity of the Omicron spike is discussed exclusively from a structural perspective or based on immunological data reported in other manuscripts.

STAR★METHODS

Detailed methods are provided in the online version of this paper and include the following:

- KEY RESOURCES TABLE
- RESOURCE AVAILABILITY
  - Lead contact
  - Materials availability
  - Data and code availability
- EXPERIMENTAL MODEL AND SUBJECT DETAILS
  - Cell lines
- METHOD DETAILS
  - Expression and purification of SARS-CoV-2 spike
  - Cryo-EM sample preparation
  - Cryo-EM data collection, processing and structure refinement
  - Calculation of domain angles and distances and identification of domain interfaces
- QUANTIFICATION AND STATISTICAL ANALYSIS

SUPPLEMENTAL INFORMATION

Supplemental information can be found online at https://doi.org/10.1016/j.celrep.2022.110428.

REFERENCES

Adams, P.D., Afonine, P.V., Bunkoczi, G., Chen, V.B., Davis, I.W., Echols, N., Headd, J.J., Hung, L.W., Kapral, G.J., Grosse-Kunstleve, R.W., et al. (2010). PHENIX: a comprehensive Python-based system for macromolecular structure solution. Acta Crystallogr. D Biol. Crystallogr. *66*, 213–221.

Amanat, F., Thapa, M., Lei, T., Ahmed, S.M.S., Adelsberg, D.C., Carreno, J.M., Strohmeier, S., Schmitz, A.J., Zafar, S., Zhou, J.Q., et al. (2021). SARS-CoV-2 mRNA vaccination induces functionally diverse antibodies to NTD, RBD, and S2. Cell *184*, 3936–3948 e3910.

Andreano, E., Paciello, I., Piccini, G., Manganaro, N., Pileri, P., Hyseni, I., Leonardi, M., Pantano, E., Abbiento, V., Benincasa, L., et al. (2021). Hybrid immunity improves B cells and antibodies against SARS-CoV-2 variants. Nature *600*, 530–535.

Barad, B.A., Echols, N., Wang, R.Y., Cheng, Y., DiMaio, F., Adams, P.D., and Fraser, J.S. (2015). EMRinger: side chain-directed model and map validation for 3D cryo-electron microscopy. Nat. Methods *12*, 943–946.

Barnes, C.O., Jette, C.A., Abernathy, M.E., Dam, K.A., Esswein, S.R., Gristick, H.B., Malyutin, A.G., Sharaf, N.G., Huey-Tubman, K.E., Lee, Y.E., et al. (2020). SARS-CoV-2 neutralizing antibody structures inform therapeutic strategies. Nature *588*, 682–687.

Benton, D.J., Wrobel, A.G., Xu, P., Roustan, C., Martin, S.R., Rosenthal, P.B., Skehel, J.J., and Gamblin, S.J. (2020). Receptor binding and priming of the spike protein of SARS-CoV-2 for membrane fusion. Nature *588*, 327–330.

Bosch, B.J., van der Zee, R., de Haan, C.A.M., and Rottier, P.J.M. (2003). The coronavirus spike protein is a class I virus fusion protein: structural and functional characterization of the fusion core complex. J. Virol. *77*, 8801–8811.

Brouwer, P.J.M., Caniels, T.G., van der Straten, K., Snitselaar, J.L., Aldon, Y., Bangaru, S., Torres, J.L., Okba, N.M.A., Claireaux, M., Kerster, G., et al. (2020). Potent neutralizing antibodies from COVID-19 patients define multiple targets of vulnerability. Science *369*, 643–650.

Burki, T.K. (2021). Omicron variant and booster COVID-19 vaccines. Lancet Respir. Med. *10*, e17.

Cai, Y., Zhang, J., Xiao, T., Peng, H., Sterling, S.M., Walsh, R.M., Rawson, S., Rits-Volloch, S., and Chen, B. (2020). Distinct conformational states of SARS-CoV-2 spike protein. Science *369*, 1586–1592.

Callaway, E., Cyranoski, D., Mallapaty, S., Stoye, E., and Tollefson, J. (2020). The coronavirus pandemic in five powerful charts. Nature *579*, 482–483.

Cameroni, E., Saliba, C., Bowen, J.E., Rosen, L.E., Culap, K., Pinto, D., De Marco, A., Zepeda, S.K., di Iulio, J., Zatta, F., et al. (2021). Broadly neutralizing

antibodies overcome SARS-CoV-2 Omicron antigenic shift. Nature. https://doi.org/10.1038/s41586-021-04386-2.

Cao, Y., Su, B., Guo, X., Sun, W., Deng, Y., Bao, L., Zhu, Q., Zhang, X., Zheng, Y., Geng, C., et al. (2020). Potent neutralizing antibodies against SARS-CoV-2 identified by high-throughput single-cell sequencing of convalescent patients' B cells. Cell *182*, 73–84.e16. https://doi.org/10.1016/j.cell.2020.1005.1025.

Cao, Y., Wang, J., Jian, F., Xiao, T., Song, W., Yisimayi, A., Huang, W., Li, Q., Wang, P., An, R., et al. (2021). Omicron escapes the majority of existing SARS-CoV-2 neutralizing antibodies. Nature. https://doi.org/10.1038/s41586-021-04385-3.

Carreño, J.M., Alshammary, H., Tcheou, J., Singh, G., Raskin, A., Kawabata, H., Sominsky, L., Clark, J., Adelsberg, D.C., Bielak, D., et al. (2021). Activity of convalescent and vaccine serum against SARS-CoV-2 Omicron. Nature. https://doi.org/10.1038/s41586-022-04399-5.

Cerutti, G., Guo, Y., Wang, P., Nair, M.S., Wang, M., Huang, Y., Yu, J., Liu, L., Katsamba, P.S., Bahna, F., et al. (2021a). Neutralizing antibody 5-7 defines a distinct site of vulnerability in SARS-CoV-2 spike N-terminal domain. Cell Rep. *37*, 109928.

Cerutti, G., Guo, Y., Zhou, T., Gorman, J., Lee, M., Rapp, M., Reddem, E.R., Yu, J., Bahna, F., Bimela, J., et al. (2021b). Potent SARS-CoV-2 neutralizing antibodies directed against spike N-terminal domain target a single supersite. Cell Host Microbe *29*, 819–833.

Cerutti, G., Rapp, M., Guo, Y., Bahna, F., Bimela, J., Reddem, E.R., Yu, J., Wang, P., Liu, L., Huang, Y., et al. (2021c). Structural basis for accommodation of emerging B.1.351 and B.1.1.7 variants by two potent SARS-CoV-2 neutralizing antibodies. Structure *29*, 655–663.

Chen, X., Li, R., Pan, Z., Qian, C., Yang, Y., You, R., Zhao, J., Liu, P., Gao, L., Li, Z., et al. (2020). Human monoclonal antibodies block the binding of SARS-CoV-2 spike protein to angiotensin converting enzyme 2 receptor. Cell Mol. Immunol. *17*, 647–649.

Chi, X., Yan, R., Zhang, J., Zhang, G., Zhang, Y., Hao, M., Zhang, Z., Fan, P., Dong, Y., Yang, Y., et al. (2020). A neutralizing human antibody binds to the N-terminal domain of the Spike protein of SARS-CoV-2. Science *369*, 650–655.

Cucinotta, D., and Vanelli, M. (2020). WHO declares COVID-19 a pandemic. Acta Biomed. *91*, 157–160.

Davis, I.W., Murray, L.W., Richardson, J.S., and Richardson, D.C. (2004). MOLPROBITY: structure validation and all-atom contact analysis for nucleic acids and their complexes. Nucleic Acids Res. *32*, W615–W619.

Emsley, P., and Cowtan, K. (2004). Coot: model-building tools for molecular graphics. Acta Crystallogr. D Biol. Crystallogr. *60*, 2126–2132.

Gobeil, S.M.C., Janowska, K., McDowell, S., Mansouri, K., Parks, R., Stalls, V., Kopp, M.F., Manne, K., Li, D., Wiehe, K., et al. (2021). Effect of natural mutations of SARS-CoV-2 on spike structure, conformation, and antigenicity. Science *373*, eabi6226.

Grant, B.J., Rodrigues, A.P., ElSawy, K.M., McCammon, J.A., and Caves, L.S. (2006). Bio3d: An R package for the comparative analysis of protein structures. Bioinformatics *22*, 2695–2696.

Harvey, W.T., Carabelli, A.M., Jackson, B., Gupta, R.K., Thomson, E.C., Harrison, E.M., Ludden, C., Reeve, R., Rambaut, A., Consortium, C.-G.U., et al. (2021). SARS-CoV-2 variants, spike mutations and immune escape. Nat. Rev. Microbiol. *19*, 409–424.

Hoffmann, M., Kleine-Weber, H., Schroeder, S., Kruger, N., Herrler, T., Erichsen, S., Schiergens, T.S., Herrler, G., Wu, N.H., Nitsche, A., et al. (2020). SARS-CoV-2 cell entry depends on ACE2 and TMPRSS2 and is blocked by a clinically proven protease inhibitor. Cell *181*, 271–280 e278.

Ju, B., Zhang, Q., Ge, J., Wang, R., Sun, J., Ge, X., Yu, J., Shan, S., Zhou, B., Song, S., et al. (2020). Human neutralizing antibodies elicited by SARS-CoV-2 infection. Nature. https://doi.org/10.1038/s41586-41020-42380-z.

Krissinel, E., and Henrick, K. (2007). Inference of macromolecular assemblies from crystalline state. J. Mol. Biol. *372*, 774–797.

Kupferschmidt, K. (2021). Where did 'weird' Omicron come from? Science *374*, 1179.

Lan, J., He, X., Ren, Y., Wang, Z., Zhou, H., Fan, S., Zhu, C., Liu, D., Shao, B., Liu, T.-Y., et al. (2022). Structural and computational insights into the SARS-CoV-2 Omicron RBD-ACE2 interaction. bioRxiv. https://doi.org/10.1101/2022.01.03.474855.

Li, T., Xue, W., Zheng, Q., Song, S., Yang, C., Xiong, H., Zhang, S., Hong, M., Zhang, Y., Yu, H., et al. (2021). Cross-neutralizing antibodies bind a SARS-CoV-2 cryptic site and resist circulating variants. Nat. Commun. *12*, 5652.

Liu, H., Wu, N.C., Yuan, M., Bangaru, S., Torres, J.L., Caniels, T.G., van Schooten, J., Zhu, X., Lee, C.D., Brouwer, P.J.M., et al. (2020a). Cross-neutralization of a SARS-CoV-2 antibody to a functionally conserved site is mediated by avidity. Immunity *53*, 1272–1280.

Liu, L., Iketani, S., Guo, Y., Chan, J.F., Wang, M., Liu, L., Luo, Y., Chu, H., Huang, Y., Nair, M.S., et al. (2021a). Striking antibody evasion manifested by the Omicron variant of SARS-CoV-2. Nature. https://doi.org/10.1038/s41586-021-04388-0.

Liu, L., Iketani, S., Guo, Y., Chan, J.F., Wang, M., Liu, L., Luo, Y., Chu, H., Huang, Y., Nair, M.S., et al. (2021b). Striking Antibody Evasion Manifested by the Omicron Variant of SARS-CoV-2. bioRxiv. https://doi.org/10.1101/2021.12.14.472719.

Liu, L., Wang, P., Nair, M.S., Yu, J., Rapp, M., Wang, Q., Luo, Y., Chan, J.F., Sahi, V., Figueroa, A., et al. (2020b). Potent neutralizing antibodies against multiple epitopes on SARS-CoV-2 spike. Nature *584*, 450–456.

Mannar, D., Saville, J.W., Zhu, X., Srivastava, S.S., Berezuk, A.M., Tuttle, K.S., Marquez, C., Sekirov, I., and Subramaniam, S. (2021). SARS-CoV-2 Omicron variant: ACE2 binding, cryo-EM structure of spike protein-ACE2 complex and antibody evasion. bioRxiv. https://doi.org/10.1101/2021.12.19.473380.

McCallum, M., De Marco, A., Lempp, F.A., Tortorici, M.A., Pinto, D., Walls, A.C., Beltramello, M., Chen, A., Liu, Z., Zatta, F., et al. (2021a). N-terminal domain antigenic mapping reveals a site of vulnerability for SARS-CoV-2. Cell *184*, 2332–2347 e2316.

McCallum, M., Walls, A.C., Sprouse, K.R., Bowen, J.E., Rosen, L.E., Dang, H.V., De Marco, A., Franko, N., Tilles, S.W., Logue, J., et al. (2021b). Molecular basis of immune evasion by the Delta and Kappa SARS-CoV-2 variants. Science *374*, 1621–1626.

Pettersen, E.F., Goddard, T.D., Huang, C.C., Couch, G.S., Greenblatt, D.M., Meng, E.C., and Ferrin, T.E. (2004). UCSF Chimera–a visualization system for exploratory research and analysis. J. Comput. Chem. *25*, 1605–1612.

Pettersen, E.F., Goddard, T.D., Huang, C.C., Meng, E.C., Couch, G.S., Croll, T.I., Morris, J.H., and Ferrin, T.E. (2021). UCSF ChimeraX: structure visualization for researchers, educators, and developers. Protein Sci. *30*, 70–82.

Pinto, D., Park, Y.J., Beltramello, M., Walls, A.C., Tortorici, M.A., Bianchi, S., Jaconi, S., Culap, K., Zatta, F., De Marco, A., et al. (2020). Cross-neutralization of SARS-CoV-2 by a human monoclonal SARS-CoV antibody. Nature *583*, 290–295.

Planas, D., Bruel, T., Grzelak, L., Guivel-Benhassine, F., Staropoli, I., Porrot, F., Planchais, C., Buchrieser, J., Rajah, M.M., Bishop, E., et al. (2021a). Sensitivity of infectious SARS-CoV-2 B.1.1.7 and B.1.351 variants to neutralizing antibodies. Nat. Med. *27*, 917–924.

Planas, D., Saunders, N., Maes, P., Guivel-Benhassine, F., Planchais, C., Buchrieser, J., Bolland, W., Porrot, F., Staropoli, I., Lemoine, F., et al. (2021b). Considerable escape of SARS-CoV-2 Omicron to antibody neutralization. Nature. https://doi.org/10.1038/s41586-021-04389-z.

Punjani, A., and Fleet, D.J. (2021). 3D variability analysis: resolving continuous flexibility and discrete heterogeneity from single particle cryo-EM. J. Struct. Biol. *213*, 107702.

Punjani, A., Rubinstein, J.L., Fleet, D.J., and Brubaker, M.A. (2017). cryo-SPARC: algorithms for rapid unsupervised cryo-EM structure determination. Nat. Methods *14*, 290–296.

Rapp, M., Guo, Y., Reddem, E.R., Yu, J., Liu, L., Wang, P., Cerutti, G., Katsamba, P., Bimela, J.S., Bahna, F.A., et al. (2021). Modular basis for potent SARS-CoV-2 neutralization by a prevalent VH1-2-derived antibody class. Cell Rep. *35*, 108950.

Sanchez-Garcia, R., Gomez-Blanco, J., Cuervo, A., Carazo, J.M., Sorzano, C.O.S., and Vargas, J. (2021). DeepEMhancer: a deep learning solution for cryo-EM volume post-processing. Commun. Biol. *4*, 874.

Saunders, K.O., Lee, E., Parks, R., Martinez, D.R., Li, D., Chen, H., Edwards, R.J., Gobeil, S., Barr, M., Mansouri, K., et al. (2021). Neutralizing antibody vaccine for pandemic and pre-emergent coronaviruses. Nature *594*, 553–559.

Scheres, S.H. (2012). RELION: implementation of a Bayesian approach to cryo-EM structure determination. J. Struct. Biol. *180*, 519–530.

Shang, J., Wan, Y., Luo, C., Ye, G., Geng, Q., Auerbach, A., and Li, F. (2020). Cell entry mechanisms of SARS-CoV-2. Proc. Natl. Acad. Sci. U S A. *117*, 11727–11734.

Shi, R., Shan, C., Duan, X., Chen, Z., Liu, P., Song, J., Song, T., Bi, X., Han, C., Wu, L., et al. (2020). A human neutralizing antibody targets the receptor-binding site of SARS-CoV-2. Nature *584*, 120–124.

Suloway, C., Pulokas, J., Fellmann, D., Cheng, A., Guerra, F., Quispe, J., Stagg, S., Potter, C.S., and Carragher, B. (2005). Automated molecular microscopy: the new Leginon system. J. Struct. Biol. *151*, 41–60.

Suryadevara, N., Shrihari, S., Gilchuk, P., VanBlargan, L.A., Binshtein, E., Zost, S.J., Nargi, R.S., Sutton, R.E., Winkler, E.S., Chen, E.C., et al. (2021). Neutralizing and protective human monoclonal antibodies recognizing the N-terminal domain of the SARS-CoV-2 spike protein. Cell *184*, 2316–2331 e2315.

Tan, Y.Z., Baldwin, P.R., Davis, J.H., Williamson, J.R., Potter, C.S., Carragher, B., and Lyumkis, D. (2017). Addressing preferred specimen orientation in single-particle cryo-EM through tilting. Nat. Methods *14*, 793–796.

Terwilliger, T.C., Sobolev, O.V., Afonine, P.V., Adams, P.D., and Read, R.J. (2020). Improvement of cryo-EM maps by density modification. Nat. Methods *17*, 923–927.

Tian, F., Tong, B., Sun, L., Shi, S., Zheng, B., Wang, Z., Dong, X., and Zheng, P. (2021). N501Y mutation of spike protein in SARS-CoV-2 strengthens its binding to receptor ACE2. Elife *10*, e69091.

Tortorici, M.A., Beltramello, M., Lempp, F.A., Pinto, D., Dang, H.V., Rosen, L.E., McCallum, M., Bowen, J., Minola, A., Jaconi, S., et al. (2020). Ultrapotent human antibodies protect against SARS-CoV-2 challenge via multiple mechanisms. Science *370*, 950–957.

Walls, A.C., Park, Y.J., Tortorici, M.A., Wall, A., McGuire, A.T., and Veesler, D. (2020). Structure, function, and antigenicity of the SARS-CoV-2 spike glycoprotein. Cell *181*, 281–292 e286.

Wang, P., Casner, R.G., Nair, M.S., Wang, M., Yu, J., Cerutti, G., Liu, L., Kwong, P.D., Huang, Y., Shapiro, L., and Ho, D.D. (2021a). Increased resistance of SARS-CoV-2 variant P.1 to antibody neutralization. Cell Host Microbe *29*, 747–751 e744.

Wang, P., Nair, M.S., Liu, L., Iketani, S., Luo, Y., Guo, Y., Wang, M., Yu, J., Zhang, B., Kwong, P.D., et al. (2021b). Antibody resistance of SARS-CoV-2 variants B.1.351 and B.1.1.7. Nature *593*, 130–135.

Wang, Q., Zhang, Y., Wu, L., Niu, S., Song, C., Zhang, Z., Lu, G., Qiao, C., Hu, Y., Yuen, K.Y., et al. (2020). Structural and functional basis of SARS-CoV-2 entry by using human ACE2. Cell *181*, 894–904 e899.

Washington, N.L., Gangavarapu, K., Zeller, M., Bolze, A., Cirulli, E.T., Schiabor Barrett, K.M., Larsen, B.B., Anderson, C., White, S., Cassens, T., et al. (2021). Emergence and rapid transmission of SARS-CoV-2 B.1.1.7 in the United States. Cell *184*, 2587–2594 e2587.

Winn, M.D., Ballard, C.C., Cowtan, K.D., Dodson, E.J., Emsley, P., Evans, P.R., Keegan, R.M., Krissinel, E.B., Leslie, A.G., McCoy, A., et al. (2011). Overview of the CCP4 suite and current developments. Acta Crystallogr. D Biol. Crystallogr. *67*, 235–242.

Wrapp, D., Wang, N., Corbett, K.S., Goldsmith, J.A., Hsieh, C.L., Abiona, O., Graham, B.S., and McLellan, J.S. (2020). Cryo-EM structure of the 2019-nCoV spike in the prefusion conformation. Science *367*, 1260–1263.

Yin, W., Xu, Y., Xu, P., Cao, X., Wu, C., Gu, C., He, X., Wang, X., Huang, S., Yuan, Q., et al. (2021). Structures of the Omicron spike trimer with ACE2 and an anti-Omicron antibody: mechanisms for the high infectivity, immune evasion and antibody drug discovery. bioRxiv. https://doi.org/10.1101/2021.12.27.474273.

Yurkovetskiy, L., Wang, X., Pascal, K.E., Tomkins-Tinch, C., Nyalile, T.P., Wang, Y., Baum, A., Diehl, W.E., Dauphin, A., Carbone, C., et al. (2020). Structural and functional analysis of the D614G SARS-CoV-2 spike protein variant. Cell *183*, 739–751 e738.

Zhang, J., Cai, Y., Xiao, T., Lu, J., Peng, H., Sterling, S.M., Walsh, R.M.J., Rits-Volloch, S., Zhu, H., Woosley, A.N., et al. (2021a). Structural impact on SARS-CoV-2 spike protein by D614G substitution. Science *372*, 525–530.

Zhang, J., Xiao, T., Cai, Y., Lavine, C.L., Peng, H., Zhu, H., Anand, K., Tong, P., Gautam, A., Mayer, M.L., et al. (2021b). Membrane fusion and immune evasion by the spike protein of SARS-CoV-2 Delta variant. Science *374*, 1353–1360.

Zhou, P., Yang, X.L., Wang, X.G., Hu, B., Zhang, L., Zhang, W., Si, H.R., Zhu, Y., Li, B., Huang, C.L., et al. (2020). A pneumonia outbreak associated with a new coronavirus of probable bat origin. Nature *579*, 270–273.

Zivanov, J., Nakane, T., and Scheres, S.H.W. (2019). A Bayesian approach to beam-induced motion correction in cryo-EM single-particle analysis. IUCrJ *6*, 5–17.

Zost, S.J., Gilchuk, P., Chen, R.E., Case, J.B., Reidy, J.X., Trivette, A., Nargi, R.S., Sutton, R.E., Suryadevara, N., Chen, E.C., et al. (2020). Rapid isolation and profiling of a diverse panel of human monoclonal antibodies targeting the SARS-CoV-2 spike protein. Nat. Med. *26*, 1422–1427.

STAR★METHODS

KEY RESOURCES TABLE

REAGENT or RESOURCE	SOURCE	IDENTIFIER
Chemicals, peptides, and recombinant proteins		
FectoPRO	Polyplus	Cat# 101000007
Expi293 Expression Media	Thermo Scientific	Cat# A14635
Opti-MEM™ Reduced Serum Media	Thermo Scientific	Cat# 31985-070
IMAC Sepharose 6 Fast Flow	GE Healthcare	Cat# 17092109
Tris Base	Thermo Scientific	Cat# BP152-5
Sodium Chloride	Thermo Scientific	Cat# S271-10
Imidazole	ACROS	Cat# 301870025
HEPES	Sigma	Cat# H3375
Critical commercial assays		
Spin Miniprep Kit	Qiagen	Cat# 27106
Hispeed Plasmid Maxi Kit	Qiagen	Cat# 12663
HisTrap Fast Flow	GE Healthcare	Cat# 17-0921-09
Ni-NTA Agarose	Thermo Scientific	Cat# R90115
Deposited data		
Cryo-EM structure of the SARS-CoV-2 spike glycoprotein Omicron B.1.1.529 variant	This paper	PDB: 7THK
Cryo-EM map of the SARS-CoV-2 spike glycoprotein Omicron B.1.1.529 variant	This paper	EMDB: EMD-25896
Experimental models: Cell lines		
Expi293F Cells	Thermo Scientific	Cat# A14527
Recombinant DNA		
pCMV3-B.1.1.1529 spike	Li et al., 2021	N/A
pαH vector	https://www.addgene.org/154754/	Cat# 154754
Software and algorithms		
Coot	Emsley and Cowtan, 2004	https://www2.mrc-lmb.cam.ac.uk/personal/pemsley/coot
cryoSPARC	Punjani et al., 2017	https://cryosparc.com
Leginon	Suloway et al., 2005	https://sbgrid.org/software/titles/leginon
Molprobity	Davis et al., 2004	http://molprobity.biochem.duke.edu
Phenix	Adams et al., 2010	https://www.phenix-online.org
The PyMOL Molecular Graphics System, Version 2.0	Schrödinger, LLC	https://pymol.org/2/support.html#page-top
RELION	Scheres, 2012	https://www3.mrc-lmb.cam.ac.uk/relion/index.php/Main_Page
DeepEMhancer	Sanchez-Garcia et al., 2021	https://github.com/rsanchezgarc/deepEMhancer
EMRinger	Barad et al., 2015	https://github.com/fraser-lab/EMRinger
UCSF Chimera	Pettersen et al., 2004	https://www.cgl.ucsf.edu/chimera/
UCSF Chimera X	Pettersen et al., 2021	https://www.cgl.ucsf.edu/chimerax/
GraphPad Prism Software	GraphPad Prism Software, Inc.	N/A
PDBePISA	Krissinel and Henrick, 2007	https://www.ebi.ac.uk/pdbe/pisa/
Python v3.8.3	Python	https://www.python.org/
The R Project for Statistical Computing	R Core Team	https://www.r-project.org/
R bio3d package	Grant et al., 2006	http://thegrantlab.org/bio3d/

RESOURCE AVAILABILITY

Lead contact

Further information and requests for resources and reagents should be directed to and will be fulfilled by the lead contact, Lawrence Shapiro (lss8@columbia.edu).

Materials availability

Expression plasmids generated in this study for expressing SARS-CoV-2 protein will be shared upon request.

Data and code availability

- Cryo-EM maps and fitted coordinates of Omicron spike have been deposited with accession code EMDB: EMD-25896 and PDB: 7THK, respectively.
- This paper does not report original code.
- Any additional information required to reanalyze the data reported in this paper is available from the lead contact upon request.

EXPERIMENTAL MODEL AND SUBJECT DETAILS

Cell lines

Expi293 cells were from ThermoFisher Scientific Inc (ThermoFisher, cat#A14527).

METHOD DETAILS

Expression and purification of SARS-CoV-2 spike

The ectodomain with 2P and furin mutations of SARS-CoV-2 B.1.1.529 trimer was synthesized, fused to an 8 × His tag at the C terminus and then cloned into the pαH vector. To purify the S trimer protein, the expression vector was transiently transfected into Expi293 cells using FectoPRO (Polyplus-transfection SA). Two days after transfection, the S trimer protein was purified using Ni-NTA resin (Invitrogen).

Cryo-EM sample preparation

The sample for cryo-EM analysis of SARS-CoV-2 S2P Omicron spike was concentrated to 0.5 mg/mL final trimer concentration. To prevent aggregation during vitrification, 0.005% (w/v) n-dodecyl β-D-maltoside was added to the sample prior to plunge freezing. Cryo-EM grids were prepared by applying 2 μL of sample to a freshly glow-discharged UltrAuFoil gold grid 0.6/1 300 mesh; the sample was vitrified in liquid ethane using a Vitrobot Mark IV with a blot time of 3 s.

Cryo-EM data collection, processing and structure refinement

Cryo-EM data were collected using the Leginon software (Suloway et al., 2005) installed on a Titan Krios electron microscope operating at 300 kV, equipped with a Gatan K3-BioQuantum direct detection device. The total dose was fractionated for 2.5 s over 50 raw frames. Processing of the first 1000 micrographs showed a slight preferred orientation in the 2D classes. The following micrographs were collected applying a 30° tilt (Tan et al., 2017). Motion correction, CTF estimation, particle picking, extraction, 2D classification, ab initio model generation, 3D classification, 3D refinements and local resolution estimation were carried out in cryoSPARC 3.2 (Punjani et al., 2017). Bayesian polishing was performed in RELION on the final particle set (Scheres, 2012; Zivanov et al., 2019). The final 3D reconstruction was obtained using non-uniform refinement with C1 symmetry, achieving a resolution of 3.1 Å. 3D variability analysis (Punjani and Fleet, 2021) was performed to confirm the absence of RBDs down conformations and to sample the mobility of the final particle set in distinct states. 3D classification using the two extremes of the variability mode did not improve the quality of the map, and the particles were merged in a consensus refinement. Particles were symmetry-expanded in C3 to produce a locally refined map using a mask built around the NTD, subsequently used to refine the NTD model and visualize most of its mutations.

The structural model of SARS-CoV-2 spike PDB entry 6VYB (Walls et al., 2020) was used as initial template for model building of the trimer. PDB entries 7EAM (Li et al., 2021) and 7L2C (Cerutti et al., 2021b) were used as initial templates to build the RBD and the NTD respectively. Automated and manual model building were iteratively performed using real space refinement in Phenix (Adams et al., 2010) and Coot (Emsley and Cowtan, 2004) respectively. Density-modified maps were produced using DeepEMhancer (Sanchez-Garcia et al., 2021) and Resolve Cryo-EM tool in Phenix (Terwilliger et al., 2020) to support manual model building. Geometry validation and structure quality assessment were performed using EMRinger (Barad et al., 2015) and Molprobity (Davis et al., 2004). Map-fitting cross correlation (Fit-in-Map tool) and figures preparation were carried out using PyMOL and UCSF Chimera (Pettersen et al., 2004) and Chimera X (Pettersen et al., 2021). A summary of the cryo-EM data collection, reconstruction and refinement statistics is shown in Table S1.

The cryo-EM structural model and maps are in the process of being deposited in the RCSB PDB and EMDB.

Calculation of domain angles and distances and identification of domain interfaces

PyMOL was used to perform the angle and distance calculations and generate plots. We superposed different spikes by aligning the S2 domain in PyMOL. For each domain, we selected a set of residues and used their $C\alpha$ for determining the center of mass of the domain. The residues used are NTD (residues 27 to 69, 80 to 130, 168 to 172, 187 to 209, 216 to 242, and 263 to 271), NTD′ (residues 44 to 53 and 272 to 293), RBD (residues 334 to 378, 389 to 443, and 503 to 521), SD1 (residues 323 to 329 and 529 to 590), SD2 (residues 294 to 322, 591 to 620, 641 to 691, and 692 to 696) (Gobeil et al., 2021). PISA was used to identify interface residues, as well as calculate buried accessible surface area and identify polar interactions (Winn et al., 2011). To identify viral mutations resulting in antibody escape, we first used PyMOL to superimpose the RBD (or NTD for analysis of anti-NTD antibodies) domains of the wildtype and Omicron variant. Omicron mutations that clash with antibodies were then identified. These results were further confirmed from the published neutralization data (Liu et al., 2021a).

QUANTIFICATION AND STATISTICAL ANALYSIS

Cryo-EM data were processed and analyzed using cryoSPARC and RELION. Cryo-EM structural statistics were analyzed with Phenix and Molprobity. Statistical details of experiments are described in method details or Figure Legends.